Journal of Magnetic Resonance **148,** 419–424 (2001)
doi:10.1006/jmre.2000.2256, available online at http://www.idealibrary.com on IDEAL®

Determination of Relative Triplet Sublevel Populating Rates during Optical Pumping Using ODMR

Andrzej Ozarowski and August H. Maki

Department of Chemistry, University of California, Davis, California 95616

Received September 5, 2000; revised November 6, 2000

A method is introduced, based on optical detection of triplet state magnetic resonance (ODMR), to determine the relative populating rates of photoexcited triplet state sublevels during optical pumping. Phosphorescence transients induced by microwave rapid passage during optical pumping are analyzed globally utilizing kinetic parameters obtained from separate microwave-induced delayed phosphorescence measurements to obtain relative sublevel populating rates. Results are unaffected by phosphorescence from triplet populations that do not yield an ODMR response. The method is applied to the triplet state of the indole chromophore in various environments to reveal the effects of local interactions on the pattern of intersystem crossing. Enhanced spin–orbit coupling effects are attributed to interactions that reduce the planar symmetry of the indole chromophore.

INTRODUCTION

The microwave-induced delayed phosphorescence (MIDP) experiment (*1*) has been used for many years to study the kinetics of photoexcited triplet state sublevels. In this method, optical pumping populates the triplet state, the excitation is terminated, and the optically detected magnetic resonance (ODMR) of the triplet state is excited by a microwave pulse or rapid passage after a time delay, but during decay of the triplet sublevel populations. Analysis of the amplitude of the "phosphorescence echo" vs the delay time allows determination of the decay kinetics of the individual sublevels. In the absence of complications from spin–lattice relaxation (SLR), the experiment can lead directly to the individual sublevel lifetimes. Over recent years we have been using an improved method for analysis of MIDP transients in which all data points contained in a digital data set consisting of either two or all three ODMR transitions are analyzed globally using a nonlinear least-squares procedure (*2*). This method yields the individual sublevel decay constants, the SLR rate constants, and the relative radiative rate constants of the triplet state. The relative sublevel populations at the point that excitation is terminated are also obtained from this analysis. The relative sublevel populating rates, p_i, $(i = x, y, z)$ could be derived *if these were the steady state populations* from the relation

$$\mathbf{p} - \mathbf{R} \cdot \mathbf{n}^0 = \mathbf{0}, \qquad [1]$$

where $\mathbf{R}$ is the rate constant matrix obtained from global MIDP analysis, $\mathbf{n}^0$ is the steady state population vector, and $\mathbf{0}$ is the null vector. In many aromatic $^3(\pi, \pi^*)$ phosphorescent states such as that of indole, the subject of this work, at least one sublevel (T_z) (z is the normal to the aromatic plane) has an extremely long lifetime because of inefficient spin–orbit coupling (SOC) with low-lying excited $^1(\pi, \pi^*)$ states (*3*, *4*). Thus, in typical MIDP experiments, the duration of the excitation period is not sufficient to achieve a true steady state and allow the application of Eq. [1]. On the other hand, a pulsed optical excitation method has been used (*5*) that yields initial sublevel populations proportional to the populating rates. Microwave saturation after a brief delay is used to probe these populations using optical detection. This method has the drawback that phosphorescence originating from triplet states not undergoing saturation introduces error. In this paper we report a new experimental method that overcomes these problem and allows the accurate determination of the relative populating rates, p_i.

THEORY AND EXPERIMENTAL METHOD

The time evolution of the excited triplet state sublevel populations in the absence of external magnetic fields is described by three coupled differential equations,

$$\frac{dn_i}{dt} = p_i - k_i n_i + w_{ij}(n_j - n_i) + w_{ik}(n_k - n_i), \qquad [2]$$

where n_i are the instantaneous populations, k_i are the rate constants for decay to the ground state, and w_{ij} is the SLR rate constant for the process $T_i \rightarrow T_j$. Since the zero field splittings are far smaller than the thermal energy, $k_B T$, we assume that $w_{ij} = w_{ji}$, etc.

Each sublevel T_i contributes $n_i k_i^r$ to the phosphorescence intensity, where k_i^r is the radiative rate constant. Thus, the phosphorescence intensity at a time t is given by

1090-7807/01 $35.00

$$I(t) = \sum_{i=1}^{3} n_i(t) k_i^{\mathrm{r}}. \qquad [3]$$

In general, both the time-dependent populations and the radiative rate constants differ significantly between the sublevels. Accordingly, transfer of population between sublevels by resonant microwaves results in transient changes in phosphorescence intensity. In the MIDP measurement, the resonant microwave pulse or rapid passage is of negligible duration relative to the sublevel lifetimes. When applied to sublevels T_i and T_j at time t', the sublevel populations are changed as follows by the resonant microwaves:

$$n_i(t') \rightarrow n_i(t') - f_{ij}[n_i(t') - n_j(t')],\ n_j(t') \rightarrow n_j(t') + f_{ij}[n_i(t') - n_j(t')],\ n_k(t') \rightarrow n_k(t'), \qquad [4]$$

where f_{ij} is the population transfer factor. $f_{ij} = \frac{1}{2}$ corresponds to equalization of n_i and n_j. The evolution of the phosphorescence intensity can be followed using Eqs. [2] and [3]. Global analysis of the transient responses yields the sets of k_i, k_i^{r}, and w_{ij} as well as the initial populations, $n_i(0)$, at the termination of excitation. Since MIDP is carried out in the absence of optical pumping, $p_i = 0$ in Eq. [2]; thus the transient responses contain no information about populating rates. These could be obtained, in principle, using Eq. [1] if the $n_i(0)$ obtained from the analysis could be equated to n_i^0. As mentioned in the previous section, this condition is difficult to achieve, and the global MIDP analysis has led often to negative values for p_z when Eq. [1] was used, indicating underpopulation of the longest lived T_z sublevel. Thus, the assumption that steady state initial populations are achieved in MIDP experiments when carried out with typical excitation periods of about 15 s (*2*) is not justified. We have designed a new experimental method analogous to MIDP, but with the microwave rapid passage applied during the excitation rather than the decay period. The transients are analyzed globally as before (*2*) but now nonzero populating rates enter directly into the kinetic expressions, Eqs. [2].

Method. Details of the ODMR spectrometer have been published previously (*2*). Samples are excited by a 100-W high-pressure mercury arc lamp filtered by a 25-cm grating monochromator with 16-nm bandwidth centered at 297 nm. The excitation path also contains a 2-mm WG 295 highpass filter and a 3-mm CS 7-54 bandpass filter. MIDP measurements are carried out at 1.2 K. Emission is monitored with a 100-cm grating monochromator with a bandwith setting of 3.2 nm. Photon counting is employed with the amplified pulses directed to a 1024 channel analyzer. The experimental cycle is 15 s of optical excitation followed by a 45-s decay period. A microwave fast passage is applied after variable delay time, t', following commencement of excitation resulting in an induced phosphorescence transient. The cycle is signal averaged for at least five periods to improve the signal/noise ratio. These timing conditions are similar to those employed previously (*2*) for MIDP of molecules such as tryptophan that have long-lived triplet states. During the decay period, the T_z sublevel does not decay completely to the ground state, retaining as much as 20% of its initial population. In order to reduce this population to insignificant levels, the $T_x \leftrightarrow T_z$ transition is continuously saturated during the decay by means of a second microwave sweeper whose output is controlled by a diode switch. Data analysis confirmed that the system was essentially in the ground state before the beginning of the subsequent excitation cycle. Both normal and "excitation" MIDP experiments were performed on each sample. Normal MIDP was analyzed globally (*2*) to obtain the kinetic and radiative parameters that were used subsequently as input parameters to fit the excitation MIDP data and extract from them the relative populating rates. Computation is essentially the same as that used in global fitting of normal MIDP data as described previously (*2*). The function

$$\chi^2 = \sum_{n=1}^{\max} \sum_{m=s(n)}^{1024} (I_{nm}^{\mathrm{meas}} - I_{nm}^{\mathrm{calc}})^2 \qquad [5]$$

is minimized with respect to the populating rates, p_i, using the Simplex method. In Eq. [5], n labels the MIDP response, while m begins with the acquisition channel $s(n)$ in which the microwave fast passage for the nth response occurs. The responses are found from Eq. [3] using momentary populations, $n_i(t)$, calculated numerically from Eqs. [2] with kinetic and radiative parameters obtained from the normal MIDP analysis. The second-order Runge–Kutta method is employed. The only fitting parameters are the populating rates and the sublevel populations at the beginning of the optical excitation. The quality of the fit is not significantly worse when the initial populations are fixed at zero.

A disadvantage of this method relative to normal MIDP is that since the measurements are made during optical pumping, fluorescence is collected along with the phosphorescence. This contributes to the level of random noise. In particular, fluctuations in the excitation source are collected in excitation MIDP experiments. We have reduced these effects in our samples by collecting the emission for both types of MIDP measurement at the peak wavelength of the most intense vibronic band of the indole derivative (ca. 0,0–1500 cm^{-1}) where the phosphorescence to fluorescence ratio is considerably larger than at the 0,0 wavelength itself. The fluorescence intensity and populating rates are assumed to be constant during the excitation period since in our experiments the depletion of the ground state population is negligible.

A series of measurements with varying t' are made on each of the three ODMR transitions, $D - E$ ($T_x \leftrightarrow T_z$), $2E$ ($T_x \leftrightarrow T_y$), and $D + E$ ($T_y \leftrightarrow T_z$). The free excitation response is

subtracted from each MIDP data set to produce curves that are close to zero for $t < t'$. The MIDP responses are normalized to the intensity of the phosphorescence at the end of the free excitation cycle. The relative p_i are normalized to unity.

Estimate of error. Since no analytical formulas are available for the derivatives of χ^2 with respect to the fitted parameters, the correlation matrix was calculated numerically. Derivatives of the phosphorescence intensity with respect to each fitted parameter, p_k, was approximated for each data point, n, as

$$\frac{\partial I_n}{\partial p_k} = [I_n(p_k + \Delta p_k) - I_n(p_k - \Delta p_k)]/2\Delta p_k.$$

Elements of the Hessian matrix, **H**, were calculated from

$$H_{kl} = \sum_{n=1}^{N} \frac{\partial I_n}{\partial p_k} \frac{\partial I_n}{\partial p_l}.$$

Standard errors in parameters were evaluated from the diagonal elements of the inverse matrix $\mathbf{C} = \mathbf{H}^{-1}$:

$$\sigma_k = (\chi^2 C_{kk}/N)^{1/2}.$$

Here, N is the number of experimental points in the global data set, ca. 15,000.

Samples. L-Tryptophan (Trp) was purchased from Fluka; yohimbine hydrochloride was from Aldrich. Polyinosinic acid, poly(I), was from Pharmacia LKB Biotechnology. NCp7, the Trp-containing nucleocapsid protein from human immunodeficiency virus type 1, was obtained from Dr. J. R. Casas-Finet at the Frederick Cancer Research and Development Center (Frederick, MD). For MIDP measurements, the aqueous solutions contained 40% by volume ethylene glycol as cryosolvent and were ca. 1 mM in the indole derivative. Yohimbine was measured both in acidic (1 mM HCl) and in basic (10 mM NaOH) solution to determine the effects of protonation. The effect of nucleic acid binding on the tryptophan residue of NCp7 was investigated by adding it to poly(I) in a 1:5 protein to nucleotide ratio.

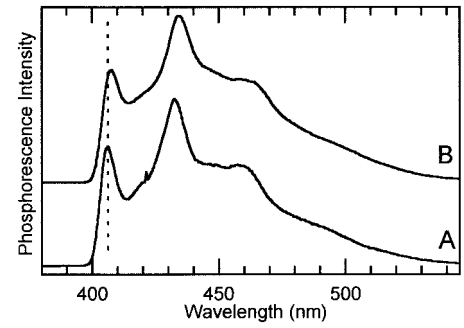

FIG. 2. Phosphorescence spectra at 4.2 K of (A) tryptophan and (B) yohimbine in 10 mM NaOH.

EXPERIMENTAL RESULTS

The molecular structure of the amino acid tryptophan that contains the indole chromophore is shown in Fig. 1A. Its phosphorescence spectrum, characterized by a well-resolved 0,0-band at 406.7 nm and a characteristic major vibronic band at 433 nm (0,0–1500 cm^{-1}), is shown in Fig. 2A. NCp7 is a nucleic acid binding protein consisting of 55 amino acids that contains two zinc finger structures (*6*), one of which includes its single Trp residue. Its phosphorescence originates from Trp and closely resembles Fig. 2A. A NMR structure reveals close association of the Trp residue of NCp7 with a guanine residue in an RNA complex (*7*). In previous ODMR studies (*8*) we found that binding of NCp7 to single stranded nucleic acids results in a phosphorescence red shift and reduction of the zero field splitting D parameter; both are characteristic of aromatic stacking interactions of Trp with a nucleobase. In this work we have investigated the effects of binding poly(I) to NCp7 on the kinetic parameters of the Trp residue. The structure of the hypoxanthine base that is present in poly(I) is shown in Fig. 1B. Previously we have shown that it stacks with Trp in NCp7–poly(I) complexes (*8*). We have also investigated yohimbine (Fig. 3) and its protonated cation. Note that yohimbine

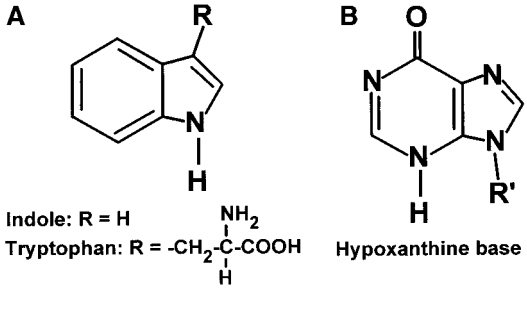

FIG. 1. (A) Structure of indole and tryptophan; (B) Structure of hypoxanthine base. In poly(I), R' represents the ribose–phosphate polymer chain.

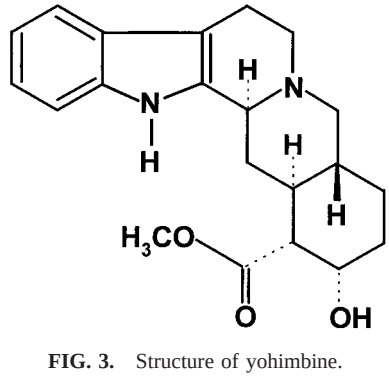

FIG. 3. Structure of yohimbine.

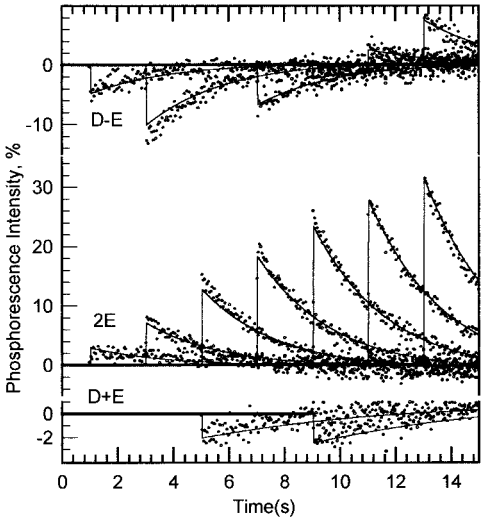

FIG. 4. "Excitation" MIDP responses of yohimbine in basic solution. The free excitation response has been subtracted from the MIDP data. The phosphorescence is monitored in the 0,0–1500 cm^{-1} band and the $D - E$ transition is saturated during the decay cycle. Data are scaled by the phosphorescence intensity at the end of the 15-s excitation period (100%). Solid lines are calculated from the kinetic data in Table 1. The signals are averaged over five cycles. Note that the vertical scale of the $D + E$ data set is expanded relative to the two other sets.

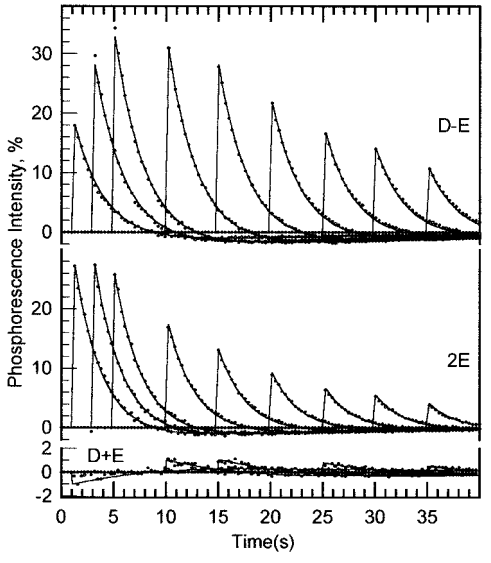

FIG. 5. Normal MIDP of yohimbine in basic solution. The free decay has been subtracted from the MIDP data. The experimental conditions are the same as in Fig. 4 except that the $D - E$ transition is not saturated during the decay. The data are scaled by the phosphorescence intensity at the end of the excitation cycle (100%). Solid lines are calculated from the kinetic data in Table 1. The signals are averaged over five cycles. The vertical scale of the $D + E$ data set is expanded relative to the others.

contains the indole chromophore (Fig. 1A) and that its phosphorescence (Fig. 2B) closely resembles that of Trp.

An example of an excitation MIDP data set for yohimbine in basic solution is shown in Fig. 4. Superimposed on the data points are the calculated MIDP responses based on the least-squares minimization with respect to the relative populating rates, as described previously. The input parameters, obtained from the normal MIDP data set measured at the same emission wavelength, are given in Table 1. The normal MIDP data set of yohimbine in basic solution is shown in Fig. 5 with the least-squares responses corresponding to the data presented in Table 1 shown as solid lines. The quality of the fit is excellent judging from the figure and from the standard error of the fitted parameters given in the table. The better signal/noise in the normal MIDP measurement is apparent from comparing Figs. 4 and 5. The data for all of the indole-containing samples that were examined are given in Table 1. There are substantial variations in the zero field splitting parameters, D and E, and the 0,0-band wavelengths, but they are not relevant in this discussion, and these data are not presented. The rate constants

TABLE 1
Kinetic and Radiative Parameters[a]

Compound[b]	k_x (s^{-1})	k_y (s^{-1})	k_z (s^{-1})	R_{zx}[c]	R_{yx}[c]	w_{xy} (s^{-1})[d]	w_{xz} (s^{-1})[d]	w_{yz} (s^{-1})[d]	p_x[e]	p_y[e]	p_z[e]
Tryptophan (407)[f]	0.306(9)	0.102(5)	0.000(1)	0.000(1)	0.128(7)	0.013(3)	0.040(5)	0.044(1)	—	—	—
Tryptophan (433)	0.314(8)	0.097(4)	0.000(3)	0.000(8)	0.153(6)	0.019(3)	0.032(4)	0.051(1)	0.431(3)	0.497(2)	0.072(1)
NCp7 (434)	0.331(7)	0.109(4)	0.004(2)	0.02(1)	0.087(6)	0.042(3)	0.027(4)	0.050(4)	0.421(5)	0.500(3)	0.078(2)
NCp7 + poly(I) (441)	0.49(2)	0.11(1)	0.000(4)	0.00(1)	0.02(1)	0.06(1)	0.05(1)	0.050(1)	0.720(5)	0.236(2)	0.043(1)
Yohimbine (436)[g]	0.32(1)	0.093(5)	0.000(3)	0.00(1)	0.06(1)	0.020(4)	0.027(5)	0.0482(3)	0.474(2)	0.433(1)	0.093(1)
Yohimbine (434)[h]	0.291(6)	0.078(3)	0.000(2)	0.000(6)	0.089(6)	0.027(2)	0.027(3)	0.0471(4)	0.425(3)	0.479(1)	0.096(1)

[a] Estimated error in the last digit given in brackets.
[b] Wavelength (nm) monitored is given in parentheses. This is the 0,0–1500 cm^{-1} band except as noted.
[c] R_{ix} is the radiative rate constant of T_i relative to T_x.
[d] w_{ij} is the $T_i \leftrightarrow T_j$ spin–lattice relaxation rate constant.
[e] Relative sublevel populating rates.
[f] Data from Ref. (*2*). 0,0-band monitored.
[g] Acidic form, 1 mM HCl.
[h] Basic form, 10 mM NaOH.

for tryptophan from this work, monitoring the strong vibronic band at 433 nm, are presented along with values from previous MIDP measurements made at the 0,0-band wavelength of 406.7 nm (*2*). The only parameter that varies significantly is $R_{yx} = k_y^r/k_x^r$, which is larger in the vibronic band emission than in the 0,0-band emission. The relative radiative rate constants are the only measured parameters that would be expected to vary with detection wavelength. The 433-nm (0,0–1500 cm^{-1}) band is largely a superposition of three active C–C stretching modes (*9*) that could alter the radiative properties of T_x and T_y.

DISCUSSION

We have employed global analysis of MIDP data acquired during optical pumping (excitation MIDP) to obtain relative sublevel-specific populating rates. In the absence of extraneous populating processes such as triplet–triplet energy transfer, these rates can be identified as relative intersystem crossing (ISC) rates.

In each case we find that >90% of ISC populates the T_x and T_y sublevels. This pattern also is reflected in the decay rate constants, where we find $k_z = 0$ within a small error for each sample (Table 1). ISC requires the mixing of singlet and triplet character in an electronic state by a perturbation such as SOC (*3, 4*). In a planar molecule, symmetry requirements allow the mixing of $^1(\pi, \pi^*)$ states only with the T_z sublevel of $^3(\pi, \pi^*)$ states by SOC (*3*). Because of the properties of the SOC Hamiltonian, however, coupling between π-electronic states is extremely weak (*4*). Thus SOC between π, π^* states and σ, π^* or π, σ^* states of differing multiplicity dominates even though the non-π electron states are at a very high energy. This interaction occurs with only the T_x and/or T_y sublevels of $^3(\pi, \pi^*)$ states, activating them in accord with our results.

For free tryptophan, basic yohimbine, and the single tryptophan residue in free NCp7, we find $p_x < p_y$ while $k_x > k_y$. These differences may reflect the fact that $S_1 \rightarrow T_1$ and $T_1 \rightarrow S_0$ involve singlet states that mix differently with $^3(\sigma, \pi^*)$ and $^3(\pi, \sigma^*)$ states. Also, a radiative contribution to the latter process could play a role.

The samples examined in this report were chosen to show the effects of specific perturbations on the triplet state kinetics of the indole chromophore. A local electric field is induced by protonation of the out-of-plane nitrogen atom of yohimbine (Fig. 3). While yohimbine in basic solution exhibits sublevel kinetics similar to those of unperturbed tryptophan, protonation causes a small but significant increase of k_x as well as a relative increase of p_x so that now $p_x > p_y$, rather than the reverse (Table 1). Much larger kinetic effects are produced in the tryptophan residue of NCp7 when the protein forms a complex with poly(I). We have shown in previous work (*8*) that phosphorescence red shifts and reduction of the ZFS of tryptophan in NCp7 upon binding with poly(I) are consistent with aromatic stacking of tryptophan with the hypoxanthine base (Fig. 1B). Here we find that the ratio p_x/p_y increases from 0.84 to 3.05 and k_x undergoes a 50% increase. Triplet–triplet energy transfer can be ruled out in the complex since this polynucleotide shows no evidence of triplet state formation (*8*), red-edge excitation insured that tryptophan was selected and, finally, it has been shown (*10*) that triplet–triplet energy transfer efficiency is severely reduced at temperatures near 1 K, essentially requiring degeneracy of donor and acceptor energies. Thus, we conclude that the effects of complex formation on the triplet state kinetics are the result of changes in internal SOC processes. The decay of T_x is selectively enhanced, and although changes in the absolute populating rates have not been determined, the relative values are consistent with the enhancement of p_x by more than a factor of 3 (assuming no changes in p_y and p_z). These observations suggest that complex formation involving aromatic stacking between tryptophan and the hypoxanthine base of poly(I) enhances the $S_1 \rightarrow T_1$ ISC and the decay of T_1 and that these enhancements work through the T_x sublevel. The principal *x*-axis is located in the plane of the indole molecule (Fig. 1A) and is approximately normal to the double bond of the five-membered ring (*11*). These changes are paralleled, but to a far lesser degree, by the effects of protonation of yohimbine.

The effects of aromatic stacking, and of local asymmetric electric fields on the kinetics of $^3(\pi, \pi^*)$ states of planar molecules, can be explained on the basis of the removal of planar symmetry. Some time ago El-Sayed *et al.* (*12*) suggested that enhancement of SOC can result from static distortions that effectively remove the symmetry plane of an aromatic molecule, allowing direct mixing of σ and π orbitals. They also used pulsed ODMR (*5*) to show that ISC selectively populates the in-plane sublevels (T_x and T_y in our coordinates) of aromatic hydrocarbons. It is reasonable that increasing the deviation from planar symmetry will induce greater SOC effects, such as enhanced ISC and shorter triplet state lifetimes. Both effects have been observed in the triplet states of aromatic charge transfer complexes in the absence of heavy atom perturbations (*13, 14*). Enhancement of ISC in proflavin when it is complexed with DNA has been observed by Lee and Galley (*15*), who suggested that an increased triplet yield may be responsible for fluorescence quenching by DNA in this system. We suggest that the stacking of the tryptophan residue of NCp7 with a hypoxanthine base of poly(I) produces an asymmetric distortion that leads to the observed kinetic effects. Charge transfer character induced in the triplet state by transannular π-electron interactions is suggested by a large reduction of the ZFS *D* parameter that is observed in the complex (*8*). Protonation of the basic nitrogen atom of yohimbine produces an electric field with an out-of-plane component that is responsible for the similar but smaller effects of reduced symmetry observed in this molecule.

It is interesting that the kinetics of the T_x sublevel are enhanced selectively by the asymmetric interactions that we have studied here, even though symmetry considerations would allow both T_x and T_y to be affected simultaneously.

ACKNOWLEDGMENTS

We thank Dr. J. R. Casas-Finet for the sample of nucleocapsid protein from HIV-1. This publication was made possible by Grant ES-02662 from the National Institute of Environmental Health Sciences, NIH. Its contents are solely the responsibility of the authors and do not necessarily represent the official views of the NIEHS, NIH.

REFERENCES

1. J. Schmidt, W. S. Veeman, and J. H. van der Waals, *Chem. Phys. Lett.* **4,** 341 (1969).
2. A. Ozarowski, J. Q. Wu, and A. H. Maki, *J. Magn. Reson. A* **121,** 178 (1996).
3. S. I. Weissman, *J. Chem. Phys.* **18,** 232 (1950).
4. D. S. McClure, *J. Chem. Phys.* **20,** 682 (1952).
5. D. A. Antheunis, J. Schmidt, and J. H. van der Waals, *Chem. Phys. Lett.* **6,** 255 (1970); H. Sixl and M. Schwoerer, *Z. Naturforsch.* **25a,** 1383 (1970).
6. J. Berg, *Science* **232,** 485 (1986).
7. R. N. De Guzman, Z. R. Wu, C. C. Stalling, L. Pappalardo, P. N. Borer, and M. F. Summers, *Science* **279,** 384 (1998).
8. J. Q. Wu, A. Ozarowski, A. H. Maki, M. A. Urbaneja, L. E. Henderson, and J. R. Casas-Finet, *Biochemistry* **36,** 12506 (1997).
9. P. R. Callis, *Methods Enzymol.* **278,** 113 (1997).
10. M. C. Prieto-Sheaffer, A. H. Maki, R. Kuimelis, and K. Nambiar, *Biochem. J.* 68, A422 (1995); M. C. Prieto, Ph. D. dissertation, Univ. of California, Davis, 1997.
11. C. A. Smith and A. H. Maki, *J. Phys. Chem.* **97,** 997 (1993).
12. M. A. El-Sayed, W. R. Moomaw, and J. B. Chodak, *Chem. Phys. Lett.* **20,** 11 (1973).
13. J. Czekalla, G. Briegleb, W. Herre, and H. J. Vahlensieck, *Z. Elektrochem.* **63,** 715 (1959).
14. N. Christodouleas and S. P. McGlynn, *J. Chem. Phys.* **40,** 166 (1964).
15. W. E. Lee and W. C. Galley, *Biophys. J.* **54,** 627 (1988).